Journal of Oceanology and Limnology

https://doi.org/10.1007/s00343-026-5534-5

Research Paper

Spatial heterogeneity of organic carbon in muddy tidal flat sediments*

Xiangxiang HE[1, 2], Cai ZHANG[1, 2], Weifang GU[3], Keyu TAO[1, 2], Yuwei LIU[1, 2], Jiawei DING[3], Xufeng YANG[1, 2], Peisong YU[1, 2, **]

[1] *State Key Laboratory of Satellite Ocean Environment Dynamics, Second Institute of Oceanography, Ministry of Natural Resources, Hangzhou 310012, China*

[2] *Key Laboratory of Marine Ecosystem Dynamics, Second Institute of Oceanography, Ministry of Natural Resources, Hangzhou 310012, China*

[3] *Marine Academy of Zhejiang Province, Hangzhou 310012, China*

Received Dec. 25, 2025; accepted in principle Feb. 5, 2026; accepted for publication Apr. 15, 2026

Abstract Muddy tidal flats (hereafter referred to as mudflats) dominate China's coastal tidal wetlands. A comprehensive assessment of their carbon stock characteristics is thus essential for refining the understanding of China's marine carbon sink capacity. In this study, sediment core sampling was conducted to systematically analyze sedimentary organic carbon (SOC) content, grain-size parameters, clay mineral composition, and carbon stock characteristics of mudflat sediments from different bays in Zhejiang Province. The results indicate that muddy sediments predominate in all three studied bays. The semi-enclosed Yanpu Bay (YP Bay), with stable hydrodynamics and small-river input, has significantly higher SOC content (0.63%±0.04%) than the high-energy Hangzhou Bay (HZ Bay) (0.55%±0.07%, large-river input) and the open Aiwan Bay (AW Bay) (0.36%±0.07%, no river input). Within individual bays, hydrodynamic conditions varied little across tidal zones, and no statistically significant differences in SOC content were detected. Nevertheless, SOC levels were generally higher in the high-tidal zone than in the middle-tidal and low-tidal zones. Analyses of total organic carbon to total nitrogen ratios (C/N) and stable carbon isotopes ($\delta^{13}C$) suggest that SOC in all three bays originates from mixed marine and terrestrial sources. Terrestrial organic matter contributes more prominently in HZ Bay and AW Bay due to the influence of Changjiang (Yangtze) River runoff, whereas YP Bay is dominated by marine-derived organic matter. By integrating data from mudflats along the Chinese coast, this study further reveals that carbon stock ranges from 18.2 to 141.5 Mg C/ha, with a total carbon storage of approximately 51.9 Tg C. The SOC stock of mudflats exhibits a "high-medium-high" spatial distribution pattern from north to south, where climate, riverine transport, and sedimentary environments are likely the primary factors driving this variation.

Keyword: mudflat; sedimentary organic carbon (SOC); SOC stock; hydrodynamic condition

1 INTRODUCTION

Coastal wetland blue carbon ecosystems traditionally include mangroves, salt marshes, and seagrass beds. These ecosystems capture and store substantial amounts of carbon through efficient plant carbon fixation and sediment carbon sequestration mechanisms (Chen et al., 2020; Pan et al., 2024), while simultaneously inhibiting carbon decomposition in anaerobic environments, thereby reducing atmospheric carbon dioxide (CO_2) concentrations and mitigating climate change. Carbon sequestered over long periods is defined as "blue carbon" (Wang et al., 2023). Globally, coastal wetland blue carbon ecosystems cover approximately 203 000 km^2, which is less than 0.5% of the total ocean area, yet they store over

* Supported by the "Pioneer" and "Leading Goose" R&D Program of Zhejiang (No. 2025C02050) and the Project of State Key Laboratory of Satellite Ocean Environment Dynamics (No. SOEDZZ2542)

** Corresponding author: yuppe@sio.org.cn

30 000 Tg C, accounting for one-third to one-half of the annual burial of carbon in global marine sediments (Mcleod et al., 2011; Duarte et al., 2013; Han et al., 2022). According to Wang et al. (2023), the total area of blue carbon ecosystems in China is estimated at approximately 14 400 km^2, with a carbon storage of about 118 Tg C (Wang et al., 2023). Of this total, vegetated blue carbon ecosystems account for roughly 33 Tg C, whereas unvegetated muddy tidal flats (mudflat) store approximately 25 to 85 Tg C. Unvegetated mudflats are widely distributed along the Chinese coast, covering an area of approximately 2 500–11 000 km^2, which is nearly three times larger than that of salt marshes. Although their primary productivity and carbon burial rates are generally lower than those of vegetated ecosystems, their extensive spatial coverage confers a substantial cumulative carbon sink potential. Consequently, mudflats have increasingly been recognized and incorporated into the framework of coastal blue carbon ecosystems (Al Disi et al., 2023; James et al., 2024).

Mudflat tidal zones are typically located adjacent to vegetated coastal wetlands, where vegetation cover generally remains below 5%. Mudflats are characterized by fine-grained sediments dominated by silt and clay, gentle slopes, and undulating microtopography (Wang et al., 2002). Such tidal flats are commonly associated with fluvial processes that deliver substantial sediment loads to coastal zones, particularly from large rivers such as the Huanghe (Yellow) River and the Changjiang (Yangtze) River (Hulskamp et al., 2023). Consequently, mudflats represent a potentially important carbon sink environment. Influenced by tidal dynamics, terrestrial runoff, adjacent vegetation, and in-situ biological processes, mudflat zones exhibit distinct ecological and environmental functions. They not only provide essential habitats for diverse organisms, but also play a critical role in hydrological regulation and pollutant purification (Passarelli et al., 2014). Recent studies further suggest that the atmospheric CO_2 absorption and sequestration potential of mudflat zones may be comparable to that of traditional vegetated blue carbon habitats, underscoring the urgent need to more fully recognize their carbon sink potential (James et al., 2024).

Mudflat ecosystems, as a critical component of the hydrological and geomorphological gradients in coastal zones, have often been treated primarily as comparative subjects in previous coastal wetland carbon sink studies—contrasted with typical blue carbon habitats such as salt marshes, mangroves, and seagrass beds (Yan et al., 2024; Zhou et al., 2024; Wu et al., 2025b). However, research specifically focusing on mudflat ecosystems remains relatively limited. In recent years, although related studies have increased (Chen et al., 2020; Guo et al., 2025a), significant uncertainties persist regarding the quantification of carbon storage in Chinese mudflat sediments. These uncertainties primarily stem from inconsistent measurement methods and substantial differences in sedimentary environments across studies (Kauffman et al., 2020). The lack of standardized and comparable datasets not only constrains robust assessments of carbon sequestration potential in unvegetated mudflats (Phang et al., 2015; Lin et al., 2020) but may also lead to systematic underestimation or overestimation of the overall carbon sink potential of coastal blue carbon ecosystems.

Compared with traditional blue carbon ecosystems, current research on the carbon sequestration capacity of mudflats has largely been confined to regional case studies, with relatively limited cross-regional comparisons. For example, Yan et al. (2024) estimated the normalized carbon storage at 1-m depth in mudflat samples from the Zhangjiang estuary (Fujian Province) to be 108.3 Mg C/ha (Yan et al., 2024), while Jin et al. (2024) reported a carbon storage of 35.5 Mg C/ha at the same depth in the Sanmen Bay mudflats (Zhejiang Province) (Jin et al., 2024). Although both sites are classified as mudflats, pronounced differences in their geographical settings and sedimentary environments exist, as further evidenced by contrasts in grain-size characteristics. Previous studies have demonstrated that bay openness and riverine inputs exert a strong control on carbon sequestration processes in mudflats (Zhang et al., 2020). Specifically, Zhang et al. (2020) reported that sedimentary soil organic carbon (SOC) content generally follows a pattern of being highest in small river estuaries, lowest in non-river estuaries, and intermediate in large river estuaries, which is closely associated with sediment clay content. Given that mudflats are strongly influenced by tidal dynamics, the mechanisms governing SOC burial may be more complex. Accordingly, this study focuses on sediment grain-size characteristics to elucidate hydrodynamic conditions under different tidal regimes and to assess their influence on carbon sequestration in mudflats.

Zhejiang Province's mudflat wetlands are regarded as one of the most important blue carbon ecosystems in China, owing to their extensive spatial coverage and high sedimentation rates (Jia et al., 2021b; Gu and Wu, 2023). Previous studies have investigated carbon storage and associated processes in mudflat wetlands within several representative bays, including Hangzhou Bay (HZ Bay), Yueqing Bay, Xiangshan Port, and Sanmen Bay (Shao et al., 2015; Chen et al., 2020; Xu et al., 2021; Jin et al., 2024; Wu et al., 2025b). However, comparative studies across different bay types remain scarce, and regional-scale variations in mudflat carbon storage have not yet been systematically clarified. Accordingly, this study focuses on three representative bay types in Zhejiang Province: (1) Yanpu Bay (YP Bay), a semi-open coastal system influenced primarily by small river inputs; (2) HZ Bay, an open coastal system strongly affected by large river inputs; and (3) Aiwan Bay (AW Bay), an open coastal system lacking direct riverine input. The objectives are to compare SOC content, source characteristics, and carbon storage among mudflat sediments across these bays, and to explore the mechanisms through which distinct bay environments regulate SOC accumulation and carbon storage. Furthermore, given the current lack of a national unified understanding of mudflat wetlands, this study will integrate SOC stock and grain size data from coastal mudflat wetlands across China to reveal spatial variations in carbon storage under different geographical settings.

2 MATERIAL AND METHOD

2.1 Study area

YP Bay is located at the southernmost tip of Cangnan County, Wenzhou City, with the study area centered at approximately 27°12′N, 120°27′E. The bay has a muddy coastline stretching 22.36 km, accompanied by an intertidal zone of 13.06 km^2 that is dominated by mudflats. YP Bay is classified as a semi-open bay, where natural barriers formed by Nanguan Island effectively attenuate wave energy.

AW Bay is located along the eastern coast of Zhejiang Province, extending from Shitang Mountain (Wenling City) to Zhantai Mountain (Yuhuan City) and connecting southward to Pishan Yang, with a semicircular coastline configuration. The bay is classified as an open bay without riverine input and is characterized by strong wave action. The study area spans the geographic range of 28°18′N–28°19′N and 121°28′E–121°32′E. AW Bay is dominated by mudflats, covering an area of approximately 57.51 km^2, and represents an important port-type tidal flat system along the eastern coast of Zhejiang Province. At present, the bay is undergoing a phase of relatively slow sedimentation, making it a suitable natural setting for investigating the carbon storage potential of mudflat sediments.

HZ Bay is located in eastern Zhejiang Province, connecting to the Qiantang River near the Zhepu area to the west, while bordered by the Zhoushan Archipelago to the east. The bay exhibits a typical funnel-shaped morphology, gradually narrowing from a wide mouth in the east toward the bay head in the west, resulting in pronounced tidal amplification and strong tidal currents. The study area is situated near Cixi city on the southern shore of HZ Bay (30°11′N–30°13′N, 121°31′E–121°32′E), one of the regions experiencing the most rapid sedimentation within the bay's intertidal flats. Influenced by substantial sediment inputs from the Changjiang River and coastal rivers in Zhejiang Province, sediment accumulation in this area is predominantly controlled by depositional processes, with sediments mainly composed of silt and clay.

2.2 Field sampling and laboratory analysis

Sediment samples were collected from two profiles in the intertidal mudflats of AW Bay and YP Bay in September 2022, followed by additional sampling in the mudflats of Cixi City, HZ Bay in May 2023 (Fig.1). Based on inundation frequency, sampling sites were categorized into high-tide, middle-tide, and low-tidal zones. A total of 18 intact vertical sediment cores (1 m in length) were collected using a non-disturbance sediment core sampler. Each core was sectioned in the field at 2-cm intervals, with care taken to preserve the integrity of the vertical sediment structure during sampling. All samples were subsequently stored at -20 °C prior to laboratory analyses. In this study, 20 samples were selected from each core for analysis, and the mean values of core parameters within each bay were used to represent the conditions of the respective bay.

Frozen sediment samples were freeze-dried, and their masses were measured before and after drying to determine water content and bulk density. Visible plant debris was manually removed from the dried samples, which were subsequently analyzed for grain size, SOC, total nitrogen (TN), and stable carbon isotope composition ($\delta^{13}C$).

For grain-size analysis, a subsample of unground sediment was dispersed in Milli-Q water with sodium hexametaphosphate added as a dispersing agent. After equilibration, the suspension was

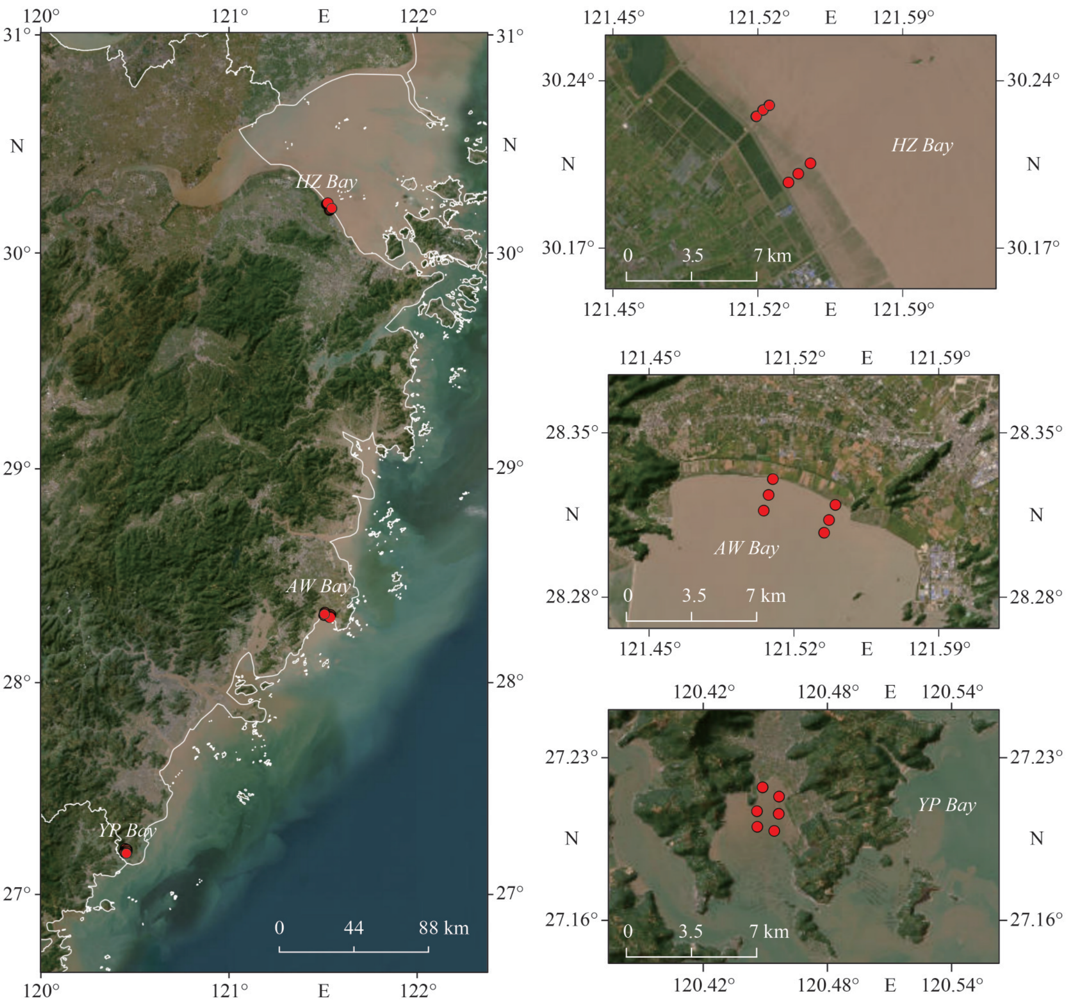

Fig.1 Map of the coastal region of Zhejiang Province showing the locations of the study areas

From north to south, the three selected bays are Hangzhou Bay (HZ Bay), Aiwan Bay (AW Bay), and Yanpu Bay (YP Bay). Red dots indicate the sediment sampling sites.

subjected to ultrasonic treatment for 5 min to achieve complete particle dispersion. Particle-size distributions were measured using a Malvern Mastersizer 3000 laser diffraction particle size analyzer. Sediment types were classified according to the Shepard classification scheme (Shepard, 1954) , and the proportions of gravel, sand, silt, and clay were calculated.

Approximately 10 g of each sample was subjected to salt washing and organic matter removal, followed by wet sieving to isolate the particle size fraction >63 μm. The remaining fraction was further processed to extract particles <2 μm in size based on Stokes' law, and oriented mounts were prepared for X-ray diffraction (XRD) analysis (Biscaye, 1965). XRD analysis was performed using an X'Pert Pro MPD powder X-ray diffractometer under the following operating parameters: CuKα radiation, tube current of 40 mA, and tube voltage of 45 kV. Three sets of oriented mounts were analyzed under different treatments: (1) natural state; (2) exposure to ethylene glycol vapor at 35 °C for 36 h; and (3) heating at 550 °C for 2 h. The scanning range was 3°–30° (2θ) with a step size of 0.02° and a step time of 0.5 s. Clay mineral identification and spectral processing were performed using Jade 6.0 software. Qualitative analysis was conducted via comprehensive comparison of the characteristic diffraction peaks of the three oriented specimens. Semi-quantitative analysis was carried out using the weighting factors proposed by Biscaye (1965) to calculate peak area ratios of clay minerals from the (001) reflections of ethylene glycol-treated samples. Smectite was identified by its 17-Å diffraction peak, Illite by its 10-Å diffraction peak, and Kaolinite and Chlorite were initially assessed using their common

7-Å diffraction peak. The relative contents of Kaolinite and Chlorite were ultimately determined from the 3.58- and 3.53-Å diffraction peaks, respectively (Biscaye, 1965). The chemical index of Illite was derived from the peak area ratio of the 5- and 10-Å diffraction peaks. Illite crystallinity was evaluated using the Kübler index, which is defined as the full width at half maximum of the 10-Å diffraction peak. Each sample was analyzed four times to obtain an average value, with the relative error controlled within 3%.

Sediment samples were ground in an agate mortar and sieved through a 100-mesh (150 μm) sieve to obtain homogenized dry ground samples. An aliquot of 0.30-g homogenized dry samples was thoroughly mixed with 1.00-mol/L hydrochloric acid (HCl) and incubated in a 55-°C water bath for 15 h to remove inorganic carbon. After acid treatment, the suspension was centrifuged at 2 000 r/min for 3 min, rinsed with Milli-Q water, and centrifuged repeatedly until neutrality was achieved. The acid-washed samples were then oven-dried at 70 °C to constant weight. Subsequently, 30 mg of the dried samples were weighed for SOC and TN content analysis using an elemental analyzer (Elementar Vario MICRO cube). Approximately 5.0 mg of acid-washed dried samples (inorganic carbon removed) was used for stable carbon isotope ($\delta^{13}C$) analysis with a Thermo Delta V Advantage stable isotope ratio mass spectrometer. The analytical precision of the instrument was ±0.1‰.

SOC storage refers to the total amount of SOC stored within a specific depth per unit area. The calculation formulas and parameter definitions are as follows:

$$BD = m_i / V_i, \quad (1)$$

$$C_S = \sum_{i=1}^{n} \overline{C_{z,i}} \times S_{A,i} \times 10^{-6}, \quad (2)$$

$$C_Z = \sum_{i=1}^{n} BD_i \times C_{org,i} \times d \times 10^2, \quad (3)$$

where BD is the bulk density of the sediment (g/cm^3), m is the dry mass of the sediment (g), V is the original sediment volume (cm^3), C_S represents the total SOC storage at a given depth (Tg C), C_Z denotes the SOC stock of the sediment column (Mg C/ha), S_A is the area of the sampling bay (ha), C_{org} is the SOC content (%), d is the sediment thickness (m), and 10 is a unit conversion factor. In this study, SOC storage calculations were standardized to a sediment depth (d) of 1 m.

2.3 Statistical analysis

Before conducting statistical analyses, the Shapiro-Wilk test and Levene's test were applied to assess data normality and homogeneity of variance, respectively. For datasets that satisfied both normality and homoscedasticity assumptions, one-way ANOVA was employed to compare the mean values of sediment properties across multiple groups (e.g., SOC contents in different bays or tidal zones). When the assumptions of normality or homogeneity of variance were violated, the non-parametric Kruskal-Wallis test was applied, which is based on rank-order comparisons of the data.

2.4 Data collection

To compile nationwide data on SOC stock in mudflat sediments, peer-reviewed studies were retrieved from the Web of Science database using the following search strategy: [("China") AND ("unvegetated flat" OR "unvegetated flats" OR "tidal wetland" OR "tidal wetlands" OR "sand flat" OR "sand flats" OR "mud flat" OR "mud flats" OR "sandflat" OR "sandflats" OR "mudflat" OR "mudflats" OR "tidal flat" OR "tidal flats" OR "intertidal flat" OR "intertidal flats") AND ("carbon sequestration" OR "carbon storage" OR "soil organic carbon" OR "carbon accumulation rate" OR "blue carbon" OR "carbon burial")]. The final literature search was conducted on 7 December 2025, yielding a total of 268 potentially relevant publications.

The retrieved literature was screened according to the following criteria: (1) only peer-reviewed journal articles were included; (2) studies were required to report SOC storage, SOC stock, SOC together with bulk density, or sediment grain size data derived from mudflat sediment cores; (3) only field-measured data were considered, whereas model-based estimates and remote sensing data were excluded. After the initial screening, further data selection was performed, focusing on SOC, grain size, SOC stock, and SOC storage data from mudflats. Studies involving vegetated tidal flats, as well as those reporting extreme outlier values, were excluded. Ultimately, data from 49 peer-reviewed articles were retained for subsequent analysis. To improve the transparency of the literature collection, screening, and data extraction process, a Preferred Reporting Items for Systematic Reviews and Meta-Analyses (PRISMA)-style flowchart of literature screening was created in this study, as shown in Supplementary Fig.S1.

3 RESULT

3.1 Sediment grain size parameters, clay minerals

The grain size composition of mudflat sediments in the three studied bays was dominated by silt and clay, although notable differences were observed among bays (Supplementary Fig.S2). In YP Bay, a semi-closed bay influenced by small river inputs, clay content was the highest (39.06%), whereas silt content was the lowest (56.50%). By contrast, AW Bay, an open bay without river input, exhibited the lowest clay content (24.17%) and the highest silt content (67.58%). HZ Bay, which is strongly influenced by large river inputs, showed intermediate clay and silt contents of 29.80% and 65.73%, respectively. Within individual bays, clay content was generally highest in the high-tide zone, whereas no significant differences in grain-size composition were observed between the mid- tide and low-tide zones (Supplementary Fig.S3). Overall, in HZ Bay and AW Bay, clay content tended to decrease while silt content increased from the high-tide zone to the low-tide zone.

The probability distributions of mean grain size (M_z) differed significantly among the three bays (Fig.2). YP Bay exhibited a peak M_z of 7.6 φ, with 93.33% of grains falling within the range of 7.1–8.1 φ. In contrast, HZ Bay had a smaller peak M_z of 7.2 φ, and 83.33% of its grains were distributed within the interval of 6.7–8.1 φ. AW Bay showed the smallest peak M_z (6.6 φ) among the three bays, with only 74.79% of grains concentrated between 6.1–7.1 φ. Notably, the M_z distributions of all three bays displayed a typical unimodal structure with a high degree of concentration.

Grain size parameters, including Skewness (S_k), Kurtosis (K_g), and sorting coefficient (σ_1), serve as robust quantitative indicators for characterizing sediment grain size properties and identifying their corresponding depositional conditions. As presented in Fig.3, the three bays (YP Bay, HZ Bay, and AW Bay) exhibited highly significant differences in S_k and K_g (P<0.01). YP Bay had a mean-S_k of 0.009, indicative of an approximately symmetric grain size distribution. By contrast, AW Bay displayed the highest positive S_k (0.178), while HZ Bay had an intermediate S_k value of 0.106. The K_g value in YP Bay was 1.163, which was significantly higher than those in HZ Bay (0.985) and AW Bay (1.004), indicating a more concentrated grain size distribution in YP Bay. The σ_1 in all three bays were greater than 1.000, with significant inter-bay differences. AW Bay showed the highest σ_1 (1.980), indicating the poorest sorting among the three bays. The differences in σ_1 among different tidal zones are relatively minor.

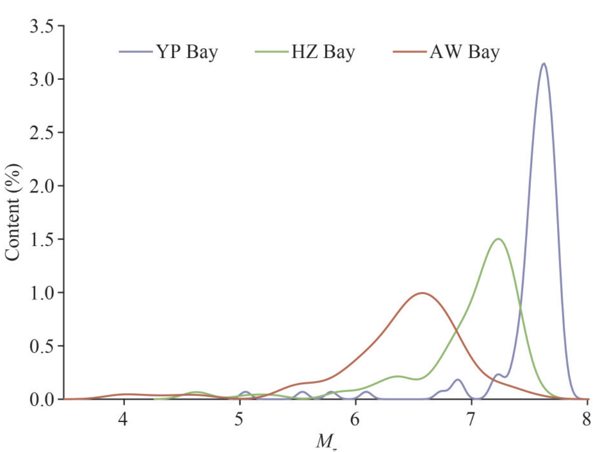

Fig.2 The probability density distribution of the mean grain size (M_z) of sediments in the three bays

A semi-quantitative analysis of clay minerals in the mudflat sediments identified Illite, Chlorite, Kaolinite, and Smectite, and their relative percentages were calculated (Supplementary Fig.S4). The percentage of Illite in clay minerals of YP Bay (60.98%) is lower than those of in HZ Bay (62.10%) and AW Bay (63.21%). YP Bay exhibited the highest concentrations of Chlorite and Kaolinite, while its Smectite content was higher than that in AW Bay but lower than that in HZ Bay. In contrast, AW Bay had the highest Illite percentage, coupled with the lowest levels of Chlorite, Kaolinite, and Smectite among the three bays. With the exception of Smectite, the relative abundances of all other clay minerals in HZ Bay were intermediate between those recorded in AW Bay and YP Bay. Both the chemical index of Illite and the Illite crystallinity index were less than 0.5 across all samples.

3.2 SOC and TN

A comparative analysis was conducted on the geochemical characteristics of mudflat sediments from YP Bay, HZ Bay, and AW Bay. The results revealed significant regional differences in SOC and TN contents among the three bays (P<0.05; Fig.4a & b). YP Bay exhibited the highest mean SOC (0.63%±0.04%) and TN (0.109%±0.010%) contents, followed by HZ Bay (SOC: 0.55%±0.07%; TN: 0.079%±0.010%), whereas AW Bay showed the lowest values (SOC: 0.36%±0.07%; TN: 0.057%±0.015%). In terms of data distribution patterns, SOC and TN values in AW Bay showed a broader range of variation,

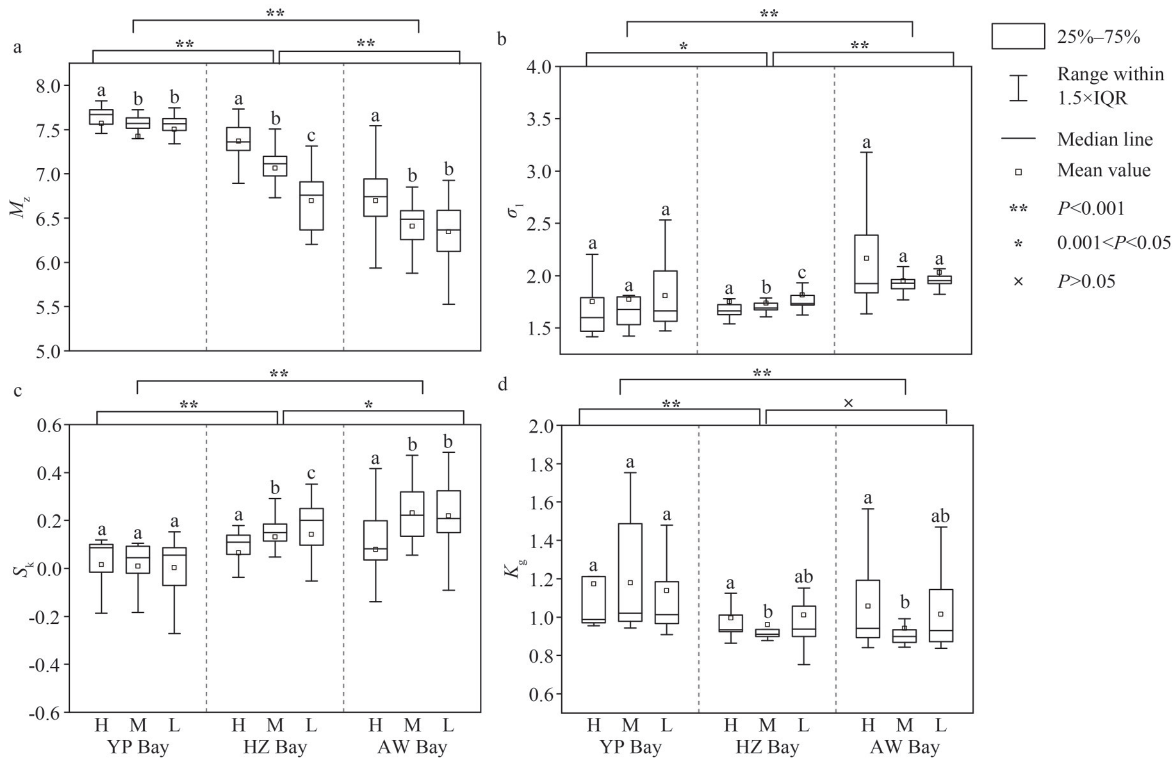

Fig.3 Distribution of various grain size parameters in the sediments of the three bays

Panels (a, b, c, and d) represent mean grain size (M_z), sorting coefficient (σ_1), Skewness (S_k), and Kurtosis (K_g), respectively. H, M, and L: high-tidal, mid-tidal, and low-tidal zones, respectively. Different letters (a, b, c) indicate significant differences (P<0.05) among the high, middle, and low tidal zones within the same bay. No significant difference is observed between tidal zones with the same letter. In the subpanels, ** indicates significant differences in parameters among the three bays (P<0.001); * indicates significant differences among the three bays (0.001<P<0.05); and × indicates no significant differences among the three bays (P>0.05). The box represents the interquartile range (IQR) from the 25th to the 75th percentile of the data, while the whiskers indicate the range of data within 1.5 times the interquartile range.

whereas those in YP Bay were relatively concentrated. The sediment C/N ratios across the three bays ranged from 4 to 10 (Fig.4c). YP Bay had the lowest C/N ratio (5.8), HZ Bay exhibited the highest value (6.8), and AW Bay showed an intermediate ratio (6.3).

Compared with the substantial differences in SOC and TN contents attributed to bay type, the variations in SOC and TN among the high-tide, mid-tide, and low-tide zones within the same bay were relatively minor (Fig.4a & b), although higher values were generally observed in the high-tidal zone. Specifically, SOC and TN contents in the high-tidal zones of AW Bay and HZ Bay were significantly higher than those in the mid-tide and low-tidal zones, whereas no significant differences were detected between the mid-tidal and low-tidal zones. In YP Bay, SOC and TN values in the high-tidal zone were slightly higher than those in the mid-tidal zone; however, differences among tidal zones were not statistically significant.

3.3 δ^{13}C

With respect to δ^{13}C values, a clear gradient was observed among the three bays, following the order: YP Bay (-22.55‰)>HZ Bay (-23.36‰)>AW Bay (-24.53‰), which is consistent with the regional variation in SOC (Fig.4d). YP Bay had the highest median δ^{13}C value, with a compact box plot and short whiskers, indicating concentrated values and low spatial variability. In contrast, HZ Bay's box plot was wider with extended whiskers, reflecting the complex influences of land-sea interactions. AW Bay exhibits the lowest median value, with the box distribution skewing toward the lower range and the whiskers extending over a wide interval, indicating a strong spatial variability in its δ^{13}C values. No significant differences in δ^{13}C values were observed among different tidal zones within the same bay.

4 DISCUSSION

4.1 The influence of particle size and clay minerals on the distribution of SOC

The stability of SOC in marine sediments is closely linked to its association with minerals, with sediment grain size being a key factor controlling

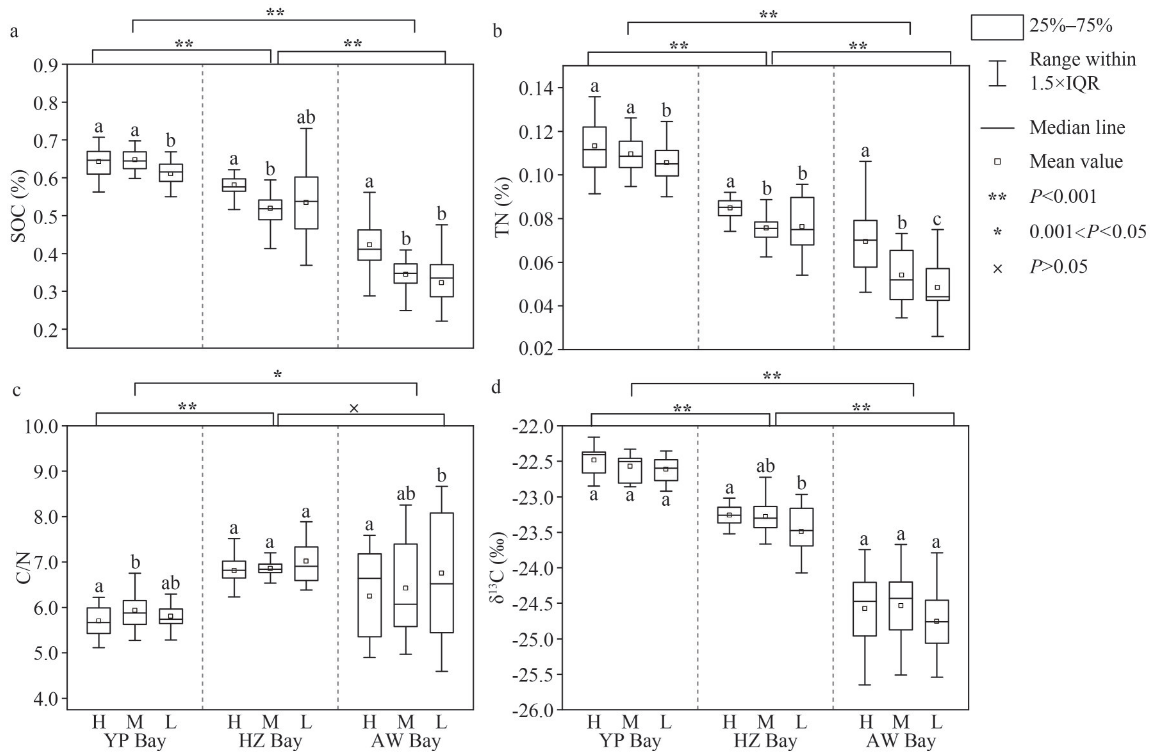

Fig.4 Distribution of carbon and nitrogen related parameters in the sediments of the three bays

a & b. the differences in sedimentary organic carbon (SOC) and total nitrogen (TN) distribution among different bays and different tidal zones; c & d. the differences in C/N and $\delta^{13}C$ distribution of sediment in the three bays. H, M, and L: high-tidal, mid-tidal, and low-tidal zones, respectively. Different letters (a, b, c) indicate significant differences ($P<0.05$) among the high, middle, and low tidal zones within the same bay. No significant difference is observed between tidal zones with the same letter. In the subpanels, ** indicates significant differences in parameters among the three bays ($P<0.001$); * indicates significant differences among the three bays ($0.001<P<0.05$); and × indicates no significant differences among the three bays ($P>0.05$). The box represents the interquartile range (IQR) from the 25th to the 75th percentile of the data, while the whiskers indicate the range of data within 1.5 times the interquartile range.

SOC preservation (Volkman et al., 2000). This study reveals significant differences in SOC content among different bay types, whereas variations within the same bay are comparatively minor relative to those observed at the regional scale. These patterns indicate that the spatial variability of SOC in mudflats is primarily controlled by regional hydrodynamic conditions, and that sediment grain size parameters can serve as effective indicators of such differences.

Previous studies have shown that SOC content is often significantly correlated with silt, clay, or muddy fractions (Zhu et al., 2011; Zhang et al., 2020; Guo et al., 2025b). This study further demonstrates that SOC is significantly positively correlated with clay content (R^2=0.746 6; Fig.5) based on an analysis of the relationships between SOC and grain size fractions across the three bays, indicating that higher clay contents are associated with higher SOC levels. Fine-grained sediments possess large specific surface areas and strong adsorption capacities, which enhance mineral–organic associations and effectively protect SOC from decomposition (Mayer, 1994a, b). Moreover, clay particles tend to flocculate in aquatic environments and preferentially settle under low-energy hydrodynamic conditions, thereby facilitating the burial and long-term preservation of organic matter (Manning and Dyer, 1999). As a result, these findings suggest that differences in sediment grain

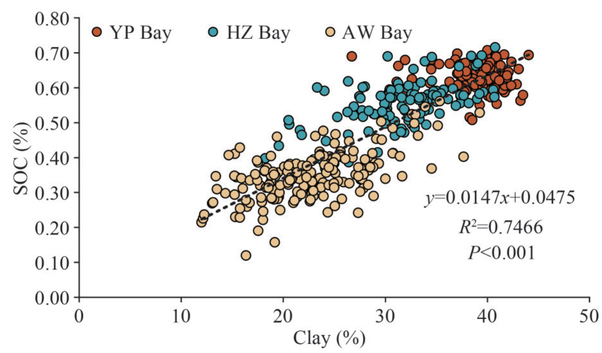

Fig.5 Relationship between sedimentary organic carbon (SOC) and clay content of mudflats

size composition play a direct and critical role in controlling the spatial distribution of SOC in mudflats.

Correlation analysis between grain-size parameters (M_z, σ_1, S_k, K_g) and SOC content in this study (Fig.6) showed that M_z and K_g were significantly and strongly positively correlated with SOC, respectively, while S_k and σ_1 were negatively correlated. These results further strengthen the link between grain-size differences and SOC. Meanwhile, grain size parameters (S_k and K_g) are effective proxies for inferring sedimentary environments: S_k reflects the symmetry of grain size distribution, while K_g quantifies the sharpness of the frequency curve peak (Fig.3). YP Bay exhibited a S_k value close to zero and a relatively high K_g, indicating a uniform grain size distribution and good sorting. In contrast, AW Bay exhibits the highest S_k value (0.102), showing a positive skew, with a relatively low K_g and the poorest sorting degree. HZ Bay showed intermediate S_k and K_g values between the two. Consistent with the above observations, σ_1 analysis revealed that YP Bay had the smallest σ_1, indicating uniform particle size and optimal sorting—reflecting relatively stable hydrodynamic conditions. As a semi-closed bay, YP Bay is sheltered by Nanguan Island. This barrier effect weakens wave action, favoring the deposition of fine particles and the accumulation of SOC. In contrast, AW Bay is an open bay lacking island shielding and riverine inputs, dominated by strong tidal and wave action, thus exhibits the maximum σ_1. These high-energy conditions inhibit clay deposition, enhance sediment coarsening, and reduce the capacity for SOC preservation. The absence of fluvial sediment supply further promotes the offshore transport of fine particles, exacerbating sediment coarsening (Yang et al., 2017). HZ Bay is partially influenced by the sheltering effect of the Zhoushan Archipelago, which weakens wave action to some extent; however, tidal dynamics remain strong. Coupled with substantial sediment inputs from large rivers, its sediment grain size characteristics and SOC preservation capacity are intermediate between those of YP Bay and AW Bay.

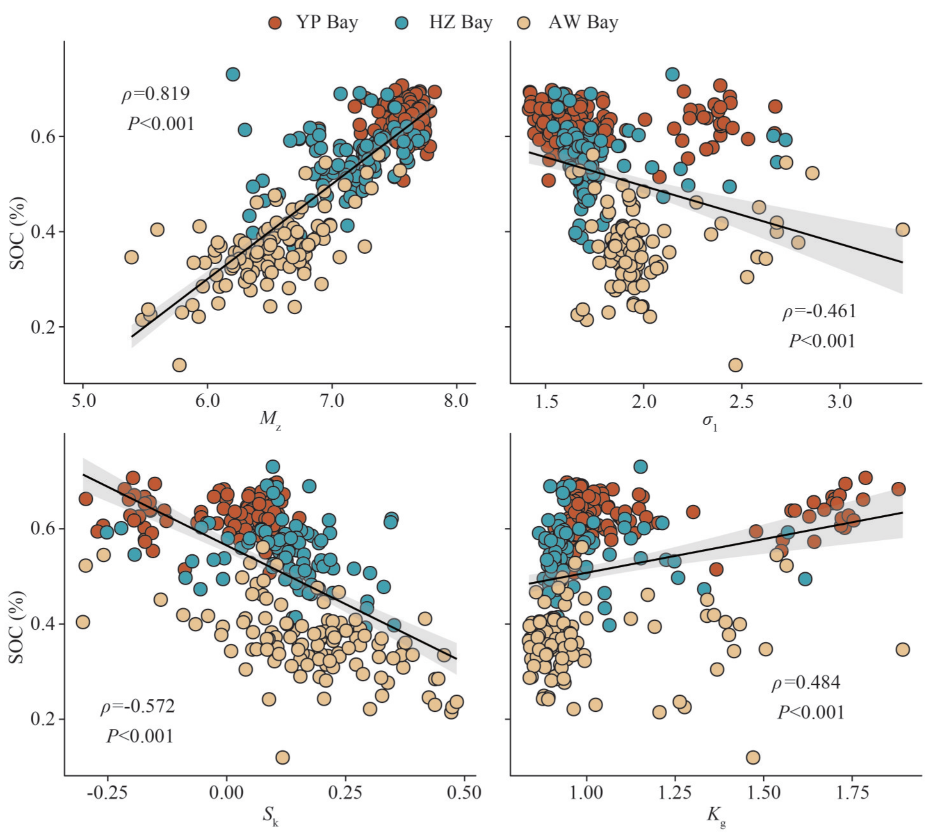

Fig.6 Correlation analysis between grain size parameters and sedimentary organic carbon (SOC) in the sediments of the three Bays

a, b, c, and d. the Spearman's correlation analysis between SOC and mean grain size (M_z), sorting coefficient (σ_1), Skewness (S_k), and Kurtosis (K_g), respectively.

When plotted on the Pejrup (1988) ternary diagram (Fig.7) (Pejrup, 1988), sediment samples from all three bays fall within the C-III and D-III fields, indicating medium to strong hydrodynamic conditions. Among them, AW Bay exhibited the strongest hydrodynamic conditions, while YP Bay showed the weakest—consistent with the inferences from the aforementioned grain size parameters.

The clay mineral assemblages in the three bays mainly consist of Illite-Chlorite-Kaolinite-Smectite, which is consistent with previous findings from HZ Bay (Xi et al., 2016), suggesting a potential influence of sediment input from the Changjiang River (Fig.7) (Xi et al., 2016). The Illite chemical index<0.5 and low crystallinity values across all three bays indicate that physical weathering is the dominant driver of sediment weathering within these bays. Additionally, clay minerals with distinct grain sizes and densities correspond to different hydrodynamic sedimentary environments (Tan et al., 2017). Illite and Chlorite exhibit good crystallinity and are characterized by coarse particle size, high density, and strong flocculation, enabling their transportation and deposition in environments with strong hydrodynamic forces. In contrast, Smectite has extremely strong water absorption and swelling properties, with extremely high dispersibility in water; it forms minimal particles and is thus more prone to deposition in environments with weak hydrodynamic conditions. Analysis using a clay mineral classification ternary diagram (Fig.7) further confirms that AW Bay has the strongest hydrodynamic conditions, while YP Bay has relatively weaker hydrodynamic environments—consistent with the conclusions from grain size data analysis. Notably, YP Bay has the highest proportion of Kaolinite. Compared with Illite and Smectite, Kaolinite forms more stable organic–mineral associations through chemical adsorption, whereas the former minerals rely more strongly on physical adsorption mechanisms. As a result, YP Bay exhibits a greater capacity for SOC stabilization and carbon sink potential than AW Bay, where strong hydrodynamic conditions constrain organic carbon preservation (Gao et al., 2018; Yang et al., 2025).

Within the same bay, the hydrodynamic intensity in the high-tide zone is attenuated, which facilitates the deposition of clay particles (Gao, 2019) and thereby enhances SOC accumulation in this zone. Consequently, SOC and TN contents are generally higher in the high-tide zone. However, due to variations in bay specific hydrodynamic conditions, the sediment distribution patterns across the high-tide, mid-tide, and low-tide zones differ among the three bays. AW Bay and HZ Bay are characterized by relatively strong hydrodynamic conditions. When tidal currents and waves propagate landward into the high-tidal zone, hydrodynamic energy is substantially attenuated, resulting in significantly higher SOC and TN contents in the high-tidal zone than in the mid-tidal and low-tidal zones. In contrast, YP Bay has overall weaker hydrodynamic conditions, with minimal variations in hydrodynamic intensity across different tidal zones. Consequently, differences in SOC and TN contents between the high-tidal zone and the mid-tidal and low-tidal zones are less pronounced in YP Bay than in AW Bay and HZ Bay.

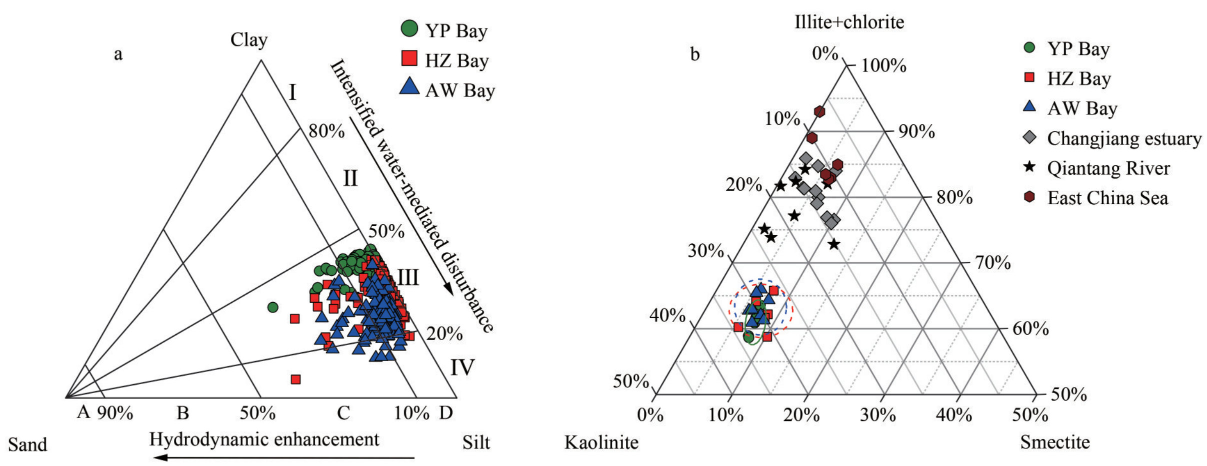

Fig.7 Grain size of sediments (a), classification of clay minerals (b) ternary figure

4.2 The source of SOC and their influencing factors

The sources of SOC in mudflat sediments can be preliminarily distinguished using the C/N ratio in combination with $\delta^{13}C$ values. It is generally accepted that marine-derived organic matter typically exhibits C/N ratios ranging from 4 to 10, whereas terrestrial-derived organic matter is characterized by much higher C/N ratios, commonly exceeding 20. In this study, C/N ratios from all three bays fall within the range of 4 to 10, indicating that the sedimentary organic matter is dominated by marine sources. The stable carbon isotope signatures further identify the sources of organic carbon. Terrestrial organic matter generally shows $\delta^{13}C$ values between approximately -33‰ and -25‰ (Hedges and Oades, 1997; Barth et al., 1998), whereas marine organic matter is typically enriched in ^{13}C, with $\delta^{13}C$ values ranging from -22‰ to -18‰ (Wada et al., 1987; Vizzini et al., 2005). The $\delta^{13}C$ values measured in this study range from -26‰ to -22‰, suggesting a mixed contribution of marine and terrestrial organic matter to SOC. To further constrain SOC source characteristics, the data were plotted on the $\delta^{13}C$-C/N mixing diagram proposed by Lamb et al. (2006) (Fig.8). The results showed that the sources in YP Bay were relatively concentrated, with more positive $\delta^{13}C$ and lower C/N values, suggesting a relatively high contribution from marine sources. By contrast, the sources in AW Bay were more scattered, with more negative $\delta^{13}C$ and higher C/N values, indicating a stronger terrestrial contribution and a more complex hydrodynamic environment.

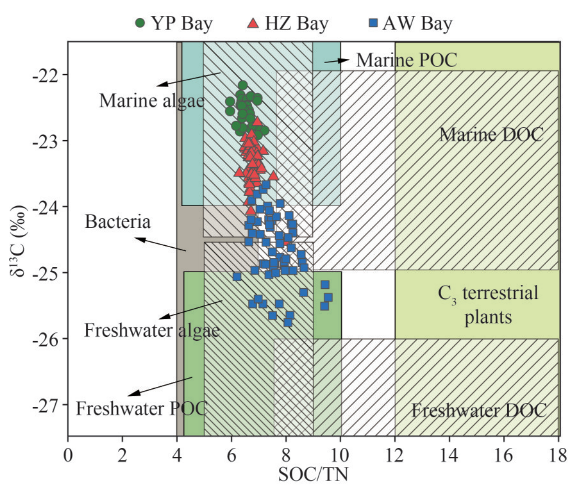

Fig.8 Source relationship figure of sedimentary organic carbon (SOC) (Lamb et al., 2006)

POC: particulate organic carbon, DOC: dissolved organic carbon.

The detailed source delineations from Lamb et al. (2006) shown in Fig.8 provide useful implications for interpreting our data. However, owing to the limited field data in this study, the detailed source classifications in the figure should be regarded as reference only.

To quantitatively estimate the relative contributions of marine- and terrestrial-derived organic matter, a two-endmember mixing model based on $\delta^{13}C$ values was applied in this study. Considering differences in bay types and riverine inputs, the $\delta^{13}C$ endmember values were set to -20.30‰ for marine organic matter and -26.50‰ for terrestrial organic matter, following previously established endmember values for Chinese coastal mudflats (Zhang et al., 2020). Model results indicate that the marine contribution in YP Bay ranges from 57.76% to 69.98%, while the terrestrial contribution ranges from 30.02% to 42.24%. In HZ Bay, the marine-derived fraction accounts for 31.65% to 60.81%, whereas the terrestrial contribution varies between 39.13% and 68.35%. In AW Bay, the marine contribution is markedly lower, ranging from 13.68% to 45.65%, while the terrestrial contribution dominates, accounting for 54.35% to 86.32%.

Spatially, Yueqing Bay acts as a geographical boundary, north of which coastal waters are strongly influenced by sediment and freshwater inputs from the Changjiang River and rivers along the Zhejiang coast (Jia et al., 2021a). HZ Bay, located adjacent to the Changjiang River estuary, therefore receives a relatively higher proportion of terrestrial-derived organic matter in its sediments (Jia et al., 2018). Although AW lacks local riverine inputs, it is still affected by diluted Changjiang River water and offshore sediments transported from the open sea. Moreover, strong hydrodynamic conditions within the bay promote the transport and deposition of relatively coarse materials. As a result, the proportion of terrestrial-derived organic matter in HZ Bay and AW Bay is higher than that in YP Bay, which lies south of Yueqing Bay and is less affected by inputs from the Changjiang River and coastal rivers, leading to a comparatively lower terrestrial contribution. Previous studies have demonstrated that sedimentary environment and grain size are key factors controlling the relative contribution of marine-derived organic matter, with finer grained sediments favoring the preservation of marine SOC (Cao et al., 2022). Consistent with these findings, YP Bay in this study has relatively stable hydrodynamic conditions and a higher proportion of fine grained sediments, leading to the strongest marine SOC preservation capacity. By comparison, the marine SOC contribution associated with HZ Bay is greater than that of AW Bay, which is consistent with differences in hydrodynamic intensity and the relative abundance of fine particulate matter between the two bays.

4.3 Carbon density of coastal sediment across the country

Using Eq.1, the sediment bulk densities of the three bays were calculated as follows: YP Bay: 1.09 g/cm^3, HZ Bay: 1.15 g/cm^3, and AW Bay: 1.34 g/cm^3. The observed differences in bulk density among the bays are closely related to variations in sediment grain size composition. Coarser sediments generally exhibit lower porosity and more efficient drainage, resulting in higher bulk densities (Xue et al., 2020). Based on Eqs.2 & 3, the average SOC stock of mudflat to a depth of 1 m was estimated to be 68.6 Mg C/ha in YP Bay, 62.6 Mg C/ha in HZ Bay, and 48.0 Mg C/ha in AW Bay. Accordingly, the total SOC storage was calculated as 8.7×10^4 Mg C for YP Bay, 4.1×10^5 Mg C for HZ Bay, and 2.7×10^5 Mg C for AW Bay. The spatial pattern of SOC stock is consistent with the distribution of SOC content, with the highest values occurring in YP Bay, the lowest in AW Bay, and intermediate values in HZ Bay. These results indicate pronounced regional differences in SOC stock capacity among mudflat ecosystems associated with different bay types.

At the national scale, previous studies have reported estimates of SOC stock in mudflats across China. To systematically evaluate the SOC stock characteristics of these environments, this study compiled SOC (n=21), grain size (n=21), and SOC stock data (n=49) from 49 relevant publications, thereby providing a comprehensive analysis of carbon storage capacity in China's coastal mudflats. The use of SOC stock as a comparative metric enhances the comparability of data across different regions. During the literature selection process, this study strictly adhered to standardized data collection protocols, thoroughly reviewing the appendices of the selected publications. Ambiguous or unqualified data were excluded, including: (1) data from vegetated tidal flats; (2) SOC data with high measurement errors; (3) data limited to surface samples only; and (4) data lacking clear specifications for sampling area type or sampling depth. Ultimately, only data from unvegetated mudflats along the Chinese coast were retained, meeting the criteria of a sampling depth of 1 m and the use of high precision analytical methods.

A synthesis of nationwide data on the grain size of mudflats indicates a positive correlation between SOC content and the mud fraction (silt and clay) (R^2=0.376 8, Fig.9), which is consistent with previous studies (Zhu et al., 2011). The three bays investigated in this study are dominated by mudflats, with SOC strongly correlated with clay content. However, the nationwide correlation is weaker than that observed at the single bay or regional scale, owing to the greater heterogeneity of tidal flat sediment types across China, including areas dominated by coarse grained sediments. Nevertheless, the trend that finer sediments are more conducive to SOC accumulation is still evident in the national dataset.

The SOC stock at a depth of 1 m in the mudflats of Zhejiang Province has been reported to range from 35.5 to 125.5 Mg C/ha, with a mean value of approximately 63.4 Mg C/ha in previous studies (Chen et al., 2020; Gu and Wu, 2023; Jin et al., 2024). In the present study, the SOC stock measured at the three mudflats sites ranged from 48.0 to 68.6 Mg C/ha, which falls within the range reported in previous studies and is close to the average value. At the national scale, SOC stock in mudflats at a depth of 1-m ranges from 18.2 to 141.5 Mg C/ha in this study, with a median value of 75.9 Mg C/ha. Xia et al. (2022) reported SOC stock in Chinese mudflats ranging from 40 to 200 Mg C/ha, whereas Chen et al. (2020), after excluding the influence of vegetation such as mangroves, reported a narrower range of 22–85 Mg C/ha. Compared with global data, Wang et al. (2026) estimated that the SOC stock of unvegetated mudflats ranged from 0.5 to 514.2 Mg C/ha, with a median of 95.7 Mg C/ha.

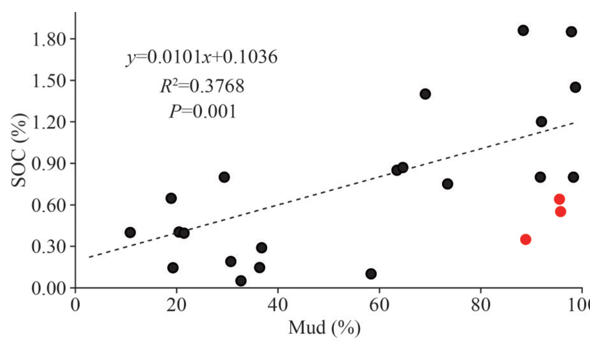

Fig.9 Relationship between sedimentary organic carbon (SOC) and mud content of coastal mudflats across the country (n=24)

Red dots indicate data points from this study.

Relative to typical global unvegetated mudflats, the coastal mudflats in China exhibit a moderate level of SOC stock, similar to that reported for Ganghwa Island, Republic of Korea (70.3 Mg C/ha) (Lee et al., 2021), but lower than that of tropical mudflats in Southeast Asia, such as the Mekong Delta (144.0 Mg C/ha) (Dung et al., 2016). Although no direct SOC stock value is available for the Wadden Sea tidal flats—one of the largest wetland systems in the world—their carbon density (<0.01 g/cm^3) suggests SOC stock comparable to or even lower than that in China (Slob et al., 2016; Chen et al., 2020). China is one of the countries with the largest area of mudflats in the world (Murray et al., 2019). Although its SOC stock per unit area is at a moderate global level, the vast distribution area renders its overall carbon burial potential and carbon sink function cannot be ignored.

The data compiled in this study is slightly lower than the results reported in some previous studies, which may be related to differences in SOC determination and analysis among different studies. The main aspects are as follows: First, incorporating sediment data from adjacent salt marshes or mangroves into mudflat datasets can overestimate SOC stocks by 30%–50% (Chen et al., 2020). Second, extrapolating surface or shallow-depth measurements to 1-m introduces systematic overestimation. Third, using of the loss-on-ignition (LOI) method, which is less accurate in low-SOC environments and requires uncertain empirical conversions (Huang et al., 2009; Thura et al., 2023). Fourth, existing databases are biased toward high-sedimentation and high-SOC bays, underrepresenting low-SOC or sparsely sampled regions—a bias amplified in national-scale extrapolations. To ensure data quality, we applied strict screening criteria, excluding potentially biased or unclear datasets. We omitted studies from vegetated tidal flats, those using the LOI method, those limited to surface samples, and those lacking clear sampling depth or environmental context. Consequently, our final dataset is robust, comprising only unvegetated muddy tidal flats along the Chinese coast, sampled to 1-m depth and analyzed with high-precision methods.

Spatially, the SOC stock of mudflats exhibits a “high-medium-high” spatial distribution pattern from north to south (Fig.10; Supplementary Table S1). SOC stocks are notably low within the latitudinal range of 30°N–35°N (e.g., Shanghai and Jiangsu),

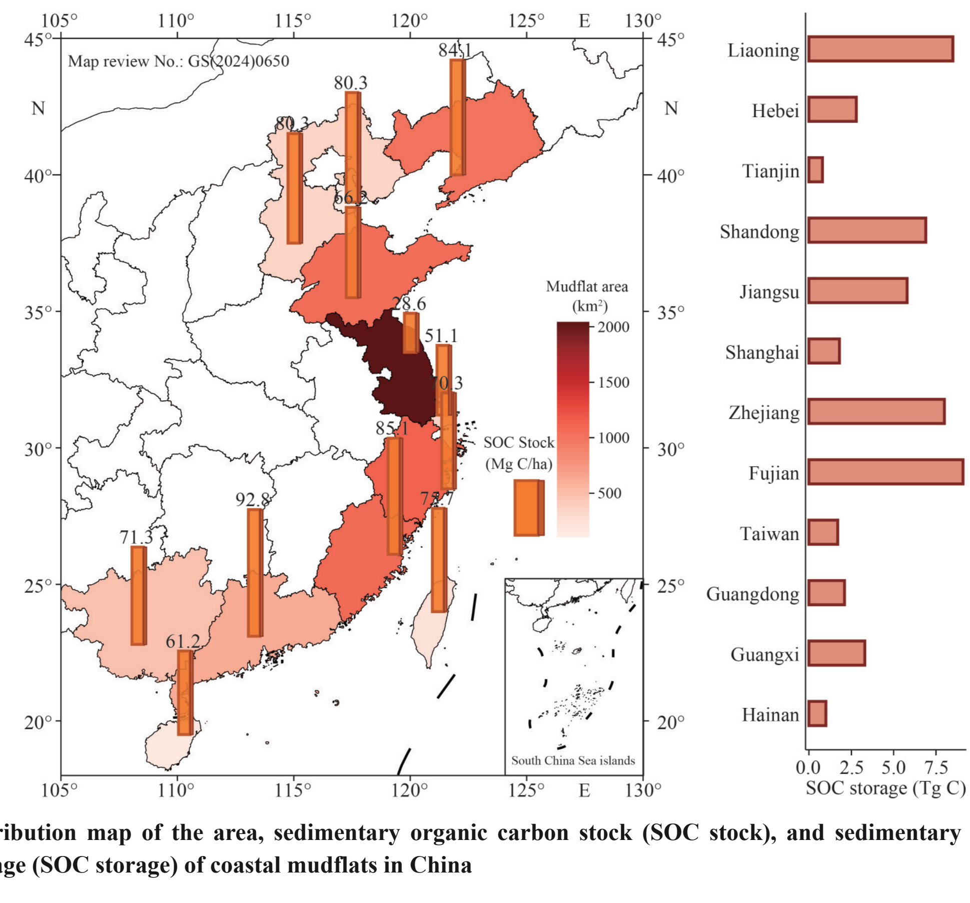

Fig.10 Distribution map of the area, sedimentary organic carbon stock (SOC stock), and sedimentary organic carbon storage (SOC storage) of coastal mudflats in China

while values gradually increase toward both the northern and southern coastal regions. The relatively high SOC stock in northern coastal areas is primarily attributed to substantial sediment inputs from estuaries, such as the transport of SOC-rich fine particles by the Liaohe River (Chen et al., 2020). Simultaneously, the low temperatures in northern regions effectively inhibit the decomposition of SOC (Wu et al., 2025a), which may also contribute to the high carbon density observed here. In contrast, mudflats in Jiangsu Province and Shanghai are strongly influenced by reworked ancient Huanghe River sediments from northern Jiangsu, as well as sediment regulation associated with the Three Gorges Reservoir. These factors result in a dominance of relatively coarse particles. Under strong open-sea hydrodynamic conditions, more coarse-grained sediments can be effectively transported and deposited, leading to reduced SOC content and lower SOC stock in this central coastal region. By comparison, the higher SOC stock observed in southern coastal mudflats are likely associated with tropical and subtropical climatic conditions, which favor vegetation growth, enhance biological productivity, and increase organic matter inputs. Moreover, the coupling of high temperature and abundant precipitation promotes the interaction and stabilization of organic matter with sediments (Yan et al., 2024; Guo et al., 2025a), resulting in relatively high SOC stock in regions such as Fujian and Guangdong provinces.

With the rapid economic development of coastal regions, the spatial and temporal patterns of China's coastal wetlands have undergone substantial changes. To obtain a reliable estimate of mudflat area, this study synthesized multiple existing assessments of coastal wetland extent and systematically screened them based on several criteria, including research objectives and data focus, data sources and methodologies, clarity of definitions, and the precision and accuracy of measurements. Ultimately, the dataset provided by Jia et al. (2021b) was selected, as it exclusively focuses on mudflats in China, clearly defines mudflats, explicitly excludes vegetated areas, and offers high-precision area estimates. Using Sentinel-2 remote sensing imagery and the Google Earth Engine platform, Jia et al. (2021b) quantified the spatial extent of China's coastal mudflats up to 2020 (Jia et al., 2021b). Their results indicate that Jiangsu Province (24.92%), Zhejiang Province (13.82%), and Fujian Province (13.02%) accounted for the largest proportions of mudflat area nationwide in 2020. The SOC storage capacity of mudflats is jointly determined by SOC stock and mudflat area, which together control the spatial differences in SOC storage among coastal provinces. Based on these factors, this study estimates that Fujian Province has the highest mudflat SOC storage (9.1 Tg C), followed by Liaoning Province (8.5 Tg C). In contrast, Tianjin and Hainan Province have relatively low SOC storage due to their smaller mudflat areas, with values of 0.8 and 1.0 Tg C, respectively (Fig.10). This study estimates the total SOC storage of China's coastal mudflats to be 51.9 Tg C, which is slightly lower than the 78.07 Tg C estimated by Chen et al. (2020). This discrepancy may stem from the overestimated mudflat areas used in Chen's study: Murray et al. (2019) misclassified many coastal aquaculture ponds as mudflats, leading to an overestimation of SOC storage (Murray et al., 2019; Fan and Li, 2024). Fan and Li (2024) estimated the SOC storage in China's coastal mudflats to be 65.4 Tg C, while Xia et al. (2022) calculated the total SOC storage in China's coastal wetlands to be 57.0 Tg C. The results of this study are consistent with these estimates, though some discrepancies remain. These differences may be attributed to: (1) variations in data acquisition and aggregation methods, which can introduce uncertainty between compiled datasets and field-based measurements; (2) inconsistent definitions of study targets, as some datasets may include vegetated tidal flats, thereby inflating SOC storage estimates; and (3) differences in the delineation of mudflat areas, which further propagate uncertainty in regional and national SOC stock calculations.

5 CONCLUSION

This study selected three representative bays in northern, central, and southern Zhejiang Province—YP Bay, HZ Bay, and AW Bay—to systematically investigate the distribution patterns, sources, and controlling factors of SOC in mudflats. The results demonstrate that contrasting sedimentary environments among the bays exert a strong control on SOC accumulation. YP Bay, a semi-open bay influenced by small river inputs, is characterized by relatively stable hydrodynamic conditions that favor the deposition of fine grained sediments; consequently, it exhibits the highest clay content and SOC levels among the three bays. In contrast, HZ Bay and AW Bay are open bays subject to stronger hydrodynamic forcing, which limits fine particle deposition and results in comparatively lower clay and SOC contents. This pattern is further supported by nationwide data from mudflats, indicating that fine grained sediments play a critical role in promoting SOC accumulation. Within individual bays, hydrodynamic differences among tidal zones are relatively minor, leading to no statistically significant differentiation in SOC content. Nevertheless, a consistent trend of higher SOC concentrations in the high tidal zone compared with the mid-tidal and low-tidal zones is still observed.

Based on sediment C/N ratios and $\delta^{13}C$ signatures, the SOC in the three bays originates from a mixture of marine and terrestrial sources, with pronounced differences in their relative contributions. Terrestrial organic matter contributes more prominently in HZ Bay and AW Bay due to the influence of Changjiang River runoff, whereas YP Bay is dominated by marine-derived organic matter. These results highlight the critical roles of hydrodynamic regimes and regional sediment sources in regulating SOC provenance in coastal mudflats.

At the national scale, the SOC stock of 1 m deep sediments in China's coastal mudflats ranges from 18.2 to 141.5 Mg C/ha corresponding to a total SOC storage of approximately 51.9 Tg C. The SOC stock of mudflats exhibits a "high-medium-high" spatial distribution pattern from north to south, where climate, riverine transport, and sedimentary environments are likely the primary factors driving this variation.

6 DATA AVAILABILITY STATEMENT

The original contributions presented in the study are included in the article and the supplementary material. Further inquiries can be directed to the corresponding authors.

References

Al Disi Z A, Naja K, Rajendran S et al. 2023. Variability of blue carbon storage in arid evaporitic environment of two coastal Sabkhas or mudflats. *Scientific Reports*, **13**(1): 12723, https://doi.org/10.1038/s41598-023-39762-7.

Barth J A C, Veizer J, Mayer B. 1998. Origin of particulate organic carbon in the upper St. Lawrence: isotopic constraints. *Earth and Planetary Science Letters*, **162**(1-4): 111-121, https://doi.org/10.1016/S0012-821X(98)00160-5.

Biscaye P E. 1965. Mineralogy and sedimentation of recent deep-sea clay in the Atlantic Ocean and adjacent seas and oceans. *GSA Bulletin*, **76**(7): 803-832, https://doi.org/10.1130/0016-7606(1965)76[803:Masord]2.0.Co;2.

Cao Y L, Bi R, Wang X C et al. 2022. The sources and burial of marine organic carbon in the Eastern China Marginal Seas. *Frontiers in Marine Science*, **9**: 824181, https://doi.org/10.3389/fmars.2022.824181.

Chen J, Wang D Q, Li Y J et al. 2020. The carbon stock and sequestration rate in tidal flats from coastal China. *Global Biogeochemical Cycles*, **34**(11): e2020GB006772, https://doi.org/10.1029/2020GB006772.

Duarte C M, Losada I J, Hendriks I E et al. 2013. The role of coastal plant communities for climate change mitigation and adaptation. *Nature Climate Change*, **3**(11): 961-968, https://doi.org/10.1038/nclimate1970.

Dung L V, Tue N T, Nhuan M T et al. 2016. Carbon storage in a restored mangrove forest in Can Gio Mangrove Forest Park, Mekong Delta, Vietnam. *Forest Ecology and Management*, **380**: 31-40, https://doi.org/10.1016/j.foreco.2016.08.032.

Fan B X, Li Y F. 2024. China's conservation and restoration of coastal wetlands offset much of the reclamation-induced blue carbon losses. *Global Change Biology*, **30**(1): e17039, https://doi.org/10.1111/gcb.17039.

Gao J, Jansen B, Cerli C et al. 2018. Organic matter coatings of soil minerals affect adsorptive interactions with phenolic and amino acids. *European Journal of Soil Science*, **69**(4): 613-624, https://doi.org/10.1111/ejss.12562.

Gao S. 2019. Geomorphology and sedimentology of tidal flats. *In*: Perillo G M E, Wolanski E, Cahoon D R eds. Coastal Wetlands: An Integrated Ecosystem Approach. 2nd edn. Elsevier, Amsterdam, The Netherlands. p.359-381.

Gu J L, Wu J P. 2023. Blue carbon effects of mangrove restoration in subtropics where *Spartina alterniflora* invaded. *Ecological Engineering*, **186**: 106822, https://doi.org/10.1016/j.ecoleng.2022.106822.

Guo M, Yang L, Zhang L et al. 2025a. Hydrology, vegetation, and soil properties as key drivers of soil organic carbon in coastal wetlands: a high-resolution study. *Environmental Science and Ecotechnology*, **23**: 100482, https://doi.org/10.1016/j.ese.2024.100482.

Guo X N, Song S S, Chen L Y et al. 2025b. Ecological connectivity between mangroves and seagrasses increases sediment blue carbon storage. *Estuarine*, *Coastal and Shelf Science*, **318**: 109231, https://doi.org/10.1016/j.ecss.2025.109231.

Han G X, Wang F M, Ma J et al. 2022. Blue carbon sink function, formation mechanism and sequestration potential of coastal salt marshes. *Chinese Journal of Plant Ecology*, **46**(4): 373-382, https://doi.org/10.17521/cjpe.2021.0264. (in Chinese with English abstract)

Hedges J I, Oades J M. 1997. Comparative organic geochemistries of soils and marine sediments. *Organic Geochemistry*, **27**(7-8): 319-361, https://doi.org/10.1016/S0146-6380(97)00056-9.

Huang P, Patel M, Santagata M C et al. 2009. Classification of Organic Soils. *Publication FHWA/IN/JTRP-2008/02*. *Joint Transportation Research Program*, *Indiana Department of Transportation and Purdue University*, *West Lafayette*, Indiana, https://doi.org/10.5703/1288284

314328.

Hulskamp R, Luijendijk A, Van Maren B et al. 2023. Global distribution and dynamics of muddy coasts. *Nature Communications*, **14**(1): 8259, https://doi.org/10.1038/s41467-023-43819-6.

James K, Macreadie P I, Burdett H L et al. 2024. It's time to broaden what we consider a 'blue carbon ecosystem'. *Global Change Biology*, **30**(5): e17261, https://doi.org/10.1111/gcb.17261.

Jia J, Zhang X Z, Zhou R H et al. 2021a. Sources of sediment in tidal flats off Zhejiang coast, southeast China. *Journal of Oceanology and Limnology*, **39**(4): 1245-1255, https://doi.org/10.1007/s00343-020-0179-2.

Jia J J, Gao J H, Cai T L et al. 2018. Sediment accumulation and retention of the Changjiang (Yangtze River) subaqueous delta and its distal muds over the last century. *Marine Geology*, **401**: 2-16, https://doi.org/10.1016/j.margeo.2018.04.005.

Jia M M, Wang Z M, Mao D H et al. 2021b. Rapid, robust, and automated mapping of tidal flats in China using time series Sentinel-2 images and Google Earth Engine. *Remote Sensing of Environment*, **255**: 112285, https://doi.org/10.1016/j.rse.2021.112285.

Jin L X, Yu P S, Liu C G et al. 2024. Photovoltaic power station impacts on the benthic ecosystem and sediment carbon storage in tidal flats in China. *Environmental Science & Technology*, **58**(47): 20954-20967, https://doi.org/10.1021/acs.est.4c04189

Kauffman J B, Giovanonni L, Kelly J et al. 2020. Total ecosystem carbon stocks at the marine-terrestrial interface: blue carbon of the Pacific Northwest Coast, United States. *Global Change Biology*, **26**(10): 5679-5692, https://doi.org/10.1111/gcb.15248.

Lamb A L, Wilson G P, Leng M J. 2006. A review of coastal palaeoclimate and relative sea-level reconstructions using δ^{13}C and C/N ratios in organic material. *Earth-Science Reviews*, **75**(1-4): 29-57, https://doi.org/10.1016/j.earscirev.2005.10.003.

Lee J, Kim B, Noh J et al. 2021. The first national scale evaluation of organic carbon stocks and sequestration rates of coastal sediments along the West Sea, South Sea, and East Sea of South Korea. *Science of the Total Environment*, **793**: 148568, https://doi.org/10.1016/j.scitotenv.2021.148568.

Lin W J, Wu J H, Lin H J. 2020. Contribution of unvegetated tidal flats to coastal carbon flux. *Global Change Biology*, **26**(6): 3443-3454, https://doi.org/10.1111/gcb.15107.

Manning A J, Dyer K R. 1999. A laboratory examination of floc characteristics with regard to turbulent shearing. *Marine Geology*, **160**(1-2): 147-170, https://doi.org/10.1016/S0025-3227(99)00013-4.

Mayer L M. 1994a. Relationships between mineral surfaces and organic carbon concentrations in soils and sediments. *Chemical Geology*, **114**(3-4): 347-363, https://doi.org/10.1016/0009-2541(94)90063-9.

Mayer L M. 1994b. Surface area control of organic carbon accumulation in continental shelf sediments. *Geochimica et Cosmochimica Acta*, **58**(4): 1271-1284, https://doi.org/10.1016/0016-7037(94)90381-6.

Mcleod E, Chmura G L, Bouillon S et al. 2011. A blueprint for blue carbon: toward an improved understanding of the role of vegetated coastal habitats in sequestering CO_2. *Frontiers in Ecology and the Environment*, **9**(10): 552-560, https://doi.org/10.1890/110004.

Murray N J, Phinn S R, DeWitt M et al. 2019. The global distribution and trajectory of tidal flats. *Nature*, **565**(7738): 222-225, https://doi.org/10.1038/s41586-018-0805-8.

Pan D L, Zhang S, Qin D H et al. 2024. Current structural status and optimized protection strategies for coastal blue-carbon Ecosystems in China. *Strategic Study of CAE*, **26**(6): 233-245, https://doi.org/10.15302/j-sscae-2024.06.024. (in Chinese with English abstract)

Passarelli C, Olivier F, Paterson D M et al. 2014. Organisms as cooperative ecosystem engineers in intertidal flats. *Journal of Sea Research*, **92**: 92-101, https://doi.org/10.1016/j.seares.2013.07.010.

Pejrup M. 1988. The triangular diagram used for classification of estuarine sediments: a new approach. *In*: De Boer P L, Vand Gelder A, Nio S D eds. Tide-Influenced Sedimentary Environments and Facies. Reidel Publishing Company, Dordrecht, Netherlands. p.289-300, https://doi.org/10.1007/978-94-015-7762-5_21.

Phang V X H, Chou L M, Friess D A. 2015. Ecosystem carbon stocks across a tropical intertidal habitat mosaic of mangrove forest, seagrass meadow, mudflat and sandbar. *Earth Surface Processes and Landforms*, **40**(10): 1387-1400, https://doi.org/10.1002/esp.3745.

Shao X X, Yang W Y, Wu M. 2015. Seasonal dynamics of soil labile organic carbon and enzyme activities in relation to vegetation types in Hangzhou Bay tidal flat wetland. *PLoS One*, **10**(11): e0142677, https://doi.org/10.1371/journal.pone.0142677.

Shepard F P. 1954. Nomenclature based on sand-silt-clay ratios. *Journal of Sedimentary Research*, **24**(3): 151-158, https://doi.org/10.1306/d4269774-2b26-11d7-8648000102c1865d.

Slob A F L, Geerdink T R A, Röckmann C et al. 2016. Governance of the Wadden Sea. *Marine Policy*, **71**: 325-333, https://doi.org/10.1016/j.marpol.2016.04.043.

Tan X L, Liu F Y, Hu L M et al. 2017. Evaluation of the particle sizes of four clay minerals. *Applied Clay Science*, **135**: 313-324, https://doi.org/10.1016/j.clay.2016.10.012.

Thura K, Serrano O, Gu J L et al. 2023. Mangrove restoration built soil organic carbon stocks over six decades: a chronosequence study. *Journal of Soils and Sediments*, **23**(3): 1193-1203, https://doi.org/10.1007/s11368-022-03418-2.

Vizzini S, Savona B, Caruso M et al. 2005. Analysis of stable carbon and nitrogen isotopes as a tool for assessing the environmental impact of aquaculture: a case study from the western Mediterranean. *Aquaculture International*, **13**(1): 157-165, https://doi.org/10.1007/s10499-004-9023-5.

Volkman J K, Rohjans D, Rullkötter J et al. 2000. Sources and diagenesis of organic matter in tidal flat sediments from the German Wadden Sea. *Continental Shelf*

Research, **20**(10-11): 1139-1158, https://doi.org/10.1016/S0278-4343(00)00016-9.

Wada E, Minagawa M, Mizutani H et al. 1987. Biogeochemical studies on the transport of organic matter along the Otsuchi River watershed, Japan. *Estuarine*, *Coastal and Shelf Science*, **25**(3): 321-336, https://doi.org/10.1016/0272-7714(87)90075-8.

Wang F M, Liu J H, Qin G M et al. 2023. Coastal blue carbon in China as a nature-based solution toward carbon neutrality. *The Innovation*, **4**(5): 100481, https://doi.org/10.1016/j.xinn.2023.100481.

Wang Y, Healy T, Healy J A. 2002. Definition, properties, and classification of muddy coasts. *In*: Healy T, Wang Y, Healy J A eds. Muddy Coasts of the World: Processes, Deposits and Function. Elsevier, Amsterdam, The Netherlands. p.9-18.

Wang Y P, Li C C, Peng Z L et al. 2026. Unvegetated tidal flats: a critical yet vulnerable coastal blue carbon sink. *Global Change Biology*, **32**(1): e70695, https://doi.org/10.1111/gcb.70695.

Wu L L, Song Z L, Xiao Z N et al. 2025a. Assessment of soil organic and inorganic carbon stocks in coastal salt marshes of China: key mechanisms elucidated. *Global Change Biology*, **31**(8): e70421, https://doi.org/10.1111/gcb.70421.

Wu X, Zhao X, Gu W F et al. 2025b. Comparative study on soil carbon sinks of artificial *Kandelia obovate* mangrove and *Spartina alterniflora* salt marsh in the southern Zhejiang coastal zone. *Journal of Tropical Oceanography*, **44**(1): 172-181, https://doi.org/10.11978/2024052. (in Chinese with English abstract)

Xi Y J, Shi Y X, Dai X R et al. 2016. Spatial difference and provenance of clay minerals as tracers of intertidal sediments in Hangzhou Bay. *Acta Sedimentologica Sinca*, **34**(2): 315-325, https://doi.org/10.14027/j.cnki.cjxb.2016.02.010. (in Chinese with English abstract)

Xia S P, Song Z L, Van Zwieten L et al. 2022. Storage, patterns and influencing factors for soil organic carbon in coastal wetlands of China. *Global Change Biology*, **28**(20): 6065-6085, https://doi.org/10.1111/gcb.16325.

Xu H, Feng B X, Li J L et al. 2021. Source and distribution of organic matters in tidal flat of Xiangshan Bay. *Oceanologia et Limnologia Sinica*, **52**(1): 97-105, https://doi.org/10.11693/hyhz20200400120. (in Chinese with English abstract)

Xue C F, Sheng H, Wei D Y et al. 2020. Dry bulk density analysis for inner shelf sediments of the East China Sea and its sedimentary implications. *Oceanologia et Limnologia Sinica*, **51**(5): 1093-1107, https://doi.org/10.11693/hyhz20191000200. (in Chinese with English abstract)

Yan R, Feng J X, Fu T et al. 2024. Spatial variation of organic carbon storage and aggregate sizes in the sediment of the Zhangjiang mangrove ecosystem. *Catena*, **234**: 107545, https://doi.org/10.1016/j.catena.2023.107545.

Yang H F, Yang S L, Xu K H. 2017. River-sea transitions of sediment dynamics: a case study of the tide-impacted Yangtze River estuary. *Estuarine*, *Coastal and Shelf Science*, **196**: 207-216, https://doi.org/10.1016/j.ecss.2017.07.005.

Yang W C, Wan Y H, Li Q Z et al. 2025. Secondary mineral-specific mechanisms of soil carbon sequestration: a review. *Energy Environmental Protection*, **39**(6): 51-63, https://doi.org/10.20078/j.eep.20251004. (in Chinese with English abstract)

Zhang Y S, Xiao X T, Liu D Y et al. 2020. Spatial and seasonal variations of organic carbon distributions in typical intertidal sediments of China. *Organic Geochemistry*, **142**: 103993, https://doi.org/10.1016/j.orggeochem.2020.103993.

Zhou J G, Zhang L L, Zhang J F et al. 2024. Blue carbon storage of tidal flats and salt marshes: a comparative assessment in two Chinese coastal areas. *Palaeogeography*, *Palaeoclimatology*, *Palaeoecology*, **655**: 112509, https://doi.org/10.1016/j.palaeo.2024.112509.

Zhu C, Wang Z H, Xue B et al. 2011. Characterizing the depositional settings for sedimentary organic matter distributions in the Lower Yangtze River-East China Sea Shelf System. *Estuarine*, *Coastal and Shelf Science*, **93**(3): 182-191, https://doi.org/10.1016/j.ecss.2010.08.001.

Electronic supplementary material

Supplementary material (Supplementary Table S1 and Figs.S1–S4) is available in the online version of this article at https://doi.org/10.1007/s00343-026-5534-5.